Forecasting the Operational Lifetime of Battery-Powered Electric Aircraft

Matthew A. Clarke* and Juan J. Alonso†
Stanford University, Stanford, California 94305

https://doi.org/10.2514/1.C036851

In recent years, advancements in high-energy and -power density batteries have become central to developing viable aircraft for urban air mobility. In this paper, we introduce the time-dependent aircraft performance over operational lifetime diagram, which is a means of integrating battery lifetime modeling into the assessment of all-electric aircraft meant to service commuter routes: both within polycentric metropolitan regions and between residential and commercial spaces. Four aircraft representing the major configuration classes of urban air mobility concepts were simulated under continuous operation spanning one year. The aircraft flew eight daily flights, with recharging of the battery pack occurring at the end of each flight. The behaviors exhibited by the aircraft powertrains offer more holistic perspectives on the limitations of battery-powered aircraft than other traditional, nontemporal methods. This study highlights that, depending on the vehicle configuration, range, and battery pack size, the battery life of achievable missions can fall by as much as 45%. Additionally, the findings reveal that the rate of change in an operational lifetime can range between 8 and 23 days per nautical mile flown. These findings equip air transportation network modelers with information critical to improving strategies for optimizing vehicle utility and maximizing revenue.

I. Introduction

WITHIN the aerospace sector, the notion that "time is money" presides over airlines competing to provide affordable and reliable services as well as manufacturers assembling aircraft on the factory floor. As a result, millions of dollars are spent streamlining these processes every year, including boarding and deboarding, routine maintenance, and inspection for airlines. Likewise, companies strive to accelerate the design-to-certification process of hardware systems and onboard flight software in the aircraft manufacturing domain. After all, money is made when aircraft are in the air and not parked on the tarmac.

Such undertakings are not exclusive to the commercial aircraft in service today but apply across the board to newly proposed concepts for long-range supersonic air travel and short-range intracity commuting. This paper is concerned with the latter: more specifically, the category of aircraft intended for urban air mobility (UAM), for which a concerted effort has been made to promote the use of clean technology. However, this presents several challenges because the energy and power densities of stored-energy cells pale as compared to what can be achieved through internal combustion using aviation fuel. In response, fast charging and battery swapping have been put forth as potential solutions for reducing idle times between flights. However, despite the belief that the latter (that is, swapping out a fully discharged battery pack for a charged one) can be an option for addressing the long charge times projected between flights, in practice, the repeated removal and insertion of packs can have detrimental and potentially hazardous implications, such as weakening the structural integrity of the electrical ports on the main airframe. Defective or partially connected packs can lead to scenarios of dangerously high voltages and resistances, which may cause permanent damage to the individual cells. Furthermore, combining this with the fact that most aircraft batteries comprise several modules positioned around the airframe for balancing purposes, the chances of a hazard become proportional to the number of independently connected modules. From a ground operations standpoint, this swapping ordeal could even be longer than recharging because removing battery modules around a nonconventional airframe such as an electrical vertical takeoff and landing (EVTOL) aircraft will require skilled labor. Any mishap on the ground can result in delayed service that puts passengers at an inconvenience or fatal crashes in graver circumstances. For these reasons, most EVTOL aircraft developers have opted for fixed battery packs that are recharged on board. Consequently, understanding how the continuous operation and environmental conditions impact battery health becomes crucial for predicting when routine maintenance is required.

In this paper, we examine electric aircraft operating repeated, identical flights over an extended period to gauge the market revenue potential of future service providers. The aircraft in this study are powered by battery packs comprising 18,650 (jelly-rolled cylindrical structure) lithium nickel manganese cobalt oxide cells. In addition to having high specific energy and power densities as compared to other lithium-ion cells, these cells have a larger operating window than other electrochemical cells such as lead acid. They also do not require complex infrastructure for safe operation, which is the case with molten salt cells such as sodium-nickel chloride. Nonetheless, despite being ideal for electric vehicles, the available energy within the battery diminishes with cyclic use, as demonstrated in Refs. [1–4]. The process by which cells age is divided into two mechanisms: calendar aging and cycle aging. The prior is concerned with aging with respect to time, whereas the latter refers to the deterioration of the cell due to repeated charging and discharging. In addition, performance degrades due to external environmental conditions such as ambient temperature and irreversible physical–chemical changes occurring within the cell. Of these internal processes, the major ones include resistive heat dissipation, mechanical stress due to the particle intercalation and deintercalation at the electrodes, and the growth of a solid electrolyte interphase (SEI) layer at the graphite anode.

The time-dependent aircraft performance over operational lifetime (TAPOOL) diagram was devised to assess the behavior of an all-electric aircraft's battery pack under repeated, realistic flight operations and environmental conditions. It differs from traditional approaches to assessing all-electric battery-powered aircraft used in previous works [5–11] in two fundamental ways:

1) Time dependency is introduced into the efficiency criteria of stored-energy systems.

Presented as AIAA Paper 2022-1996 at the AIAA SciTech 2022 Forum, San Diego, CA, January 3–7, 2022; received 18 February 2022; revision received 10 May 2022; accepted for publication 13 May 2022; published online 10 June 2022.

*Ph.D. Candidate, Department of Aeronautics and Astronautics. Student Member AIAA.

†Vance D. and Arlene C. Coffman Professor, Department of Aeronautics and Astronautics. Fellow AIAA.

2) The complete flight profile that includes the climb and descent stages of a mission is used rather than the constant altitude and constant airspeed assumptions in the computation of range and endurance.

Of course, this new diagram only covers a subset of novel powertrains under development today. The advent of hybrid electric technology and the assessment of its utility over extended periods must also be explored in great depth. As shown in Refs. [12,13], these systems can possess performance benefits over their all-electric counterparts. This, however, is not covered in this paper.

In this study, we employ the comprehensive model developed in previous work by Clarke and Alonso [14] for predicting the state of charge (SOC) during cycling as well as the state of health (SOH) over an extended period of use. The remainder of this paper is broken into five sections: Sec. II is a review of potential routes for UAM in U.S. cities and the market potential of this mode of transportation; Sec. III provides the geometric and powertrain specifications of the aircraft studied; Sec. IV outlines additional information about the flight profiles for each vehicle; Sec. V presents a compacted representation of findings with the aid of TAPOOL diagrams; and lastly, Sec. VI compares the methodology used in this study to a traditional, nontemporal method for estimating the endurance of battery-powered electric aircraft.

II. Urban Air Mobility and Potential Business Cases

UAM has garnered significant traction over the past decade. This can be attributed to an assortment of factors, including overburdened and undermaintained infrastructure, the lack of real estate upon which to expand roads and railways, and the rising passenger dissatisfaction stemming from traffic gridlock. Therefore, it was not a matter of if but when UAM would become part of the discussion of future transportation infrastructure within large cities worldwide. Thus far, several studies have sought to outline roadmaps for making this a reality. The fraction of them that focused on market valuation has attempted to evaluate potential use cases, determine optimum vertiport location and density, estimate total journey and wait times, quantify cost per seat mile, and forecast the point of net-positive profit, among others. More specifically, in terms of the use cases, Booz Allen Hamilton, Inc., [15] identified three that have been widely accepted as the most promising: first, last-mile delivery of packages from local distribution hubs; second, air shuttles resembling other transit options, such as buses and subways, with regularly scheduled, predetermined routes; and third, ride-sharing air taxis allowing commuters to request pickup and dropoff destinations. This report also identified the potential cities in which the first rollout of UAM operations could occur: four of which are discussed in greater detail in subsequent sections of this paper. Another study by Goyal et al. [16] used Monte Carlo simulations to study the scale of the UAM operations required to realize an annual market valuation of 2.5 billion U.S. dollars. Of course, this rollout is expected to happen in phases over some time: first, allowing market modelers to collect consumer data; and second, allowing aircraft manufacturers the opportunity to iterate vehicle design while simultaneously expanding production. Moreover, because the initial cost per mile is expected to be high, the first set of vertiports must be placed judiciously. In response, some studies have integrated gross domestic product per capita into models predicting market growth [17]. Others, such as Robinson et al. [18], have factored in climate, urban density, the number of existing airports, traffic congestion, and the presence of various economic clusters in the identification of potential locations for launching operations. One of these candidates, San Francisco, was also suggested by Antcliff et al. [19] to be an early adopter due to the high percentage of long-distance commuting from peripheral cities such as Stockton, Tracy, and San Rafael, to name a few.

From a review of these studies, a list of potential routes in four cities is provided in Table 1. Although most nodes are of existing airports listed by their three-letter geocode, there are a few that are new vertiports. These are downtown Los Angeles (DLA), lower Manhattan (LMX), New Brunswick (NBX), downtown Dallas (DLX), Denton (DDX), McKinney (MDX), and downtown Fort Worth (FWX). Routes within the table are marked as solid lines in Fig. 1, whereas other potential routes between nodes are marked as dashed lines. All distances are given in nautical miles.

Table 1 UAM destinations in four major metropolitan areas within the United States

Metropolitan area	Route	Range, n miles
San Francisco Bay metropolitan area	SFO–SJC	26
	OAK–SMF	67
	OAK–SJC	26
	PAO–OAK	17
	AFA–SFO	21
	SFO–SCK	56
New York metropolitan area	LMX[a]–JFK	10
	HVN–LGA	55
	EWF–JFK	21
	NBX[a]–LMX[a]	26
	HVN–JFK	50
	JFK–ISP	50
Los Angeles metropolitan area	LAX–SNA	31
	SBD–SNA	41
	BUR–SBD	53
	DLA[a]–LAX	10
	SNA–CLD	35
	PMD–LAX	44
Dallas–Fort Worth metropolitan area	DLX–DFW	27
	DFW–DLX[a]	13
	DFW–FWX[a]	16
	MLX[a]–DLX[a]	28
	FWX[a]–DDX[a]	37
	MLX[a]–DDX[a]	25

[a]New vertiports.

SFO = San Francisco International Airport, SJC = Norman Y. Mineta San Jose International Airport, OAK = Oakland International Airport, PAO = Palo Alto Airport, AFA = San Rafael Airport, SMF = Sacramento International Airport, SCK = Stockton Metropolitan Airport, JFK = John F. Kennedy International Airport, HVN = Tweed New Haven Airport, LGA = LaGuardia Airport, ISP = MacArthur Airport, LAX = Los Angeles International Airport, SBD = San Bernardino International Airport, SNA = John Wayne Airport, BUR = Hollywood Burbank Airport, CLD = McClellan-Palomar Airport, PMD = Palmdale Regional Airport, DFW = Dallas Fort Worth International Airport.

Apart from the public acceptance, issues concerning aircraft noise, pilot training, the degree of autonomy in the flight controls, and the maturity of stored-energy systems still linger. These aspects are all closely tracked by investors betting on significant returns on their investments. Regulatory agencies are also tracking these technical domains that, to varying degrees, all impact the built and natural environments. Under the microscope in this study is the operation of lithium-ion batteries subjected to realistic loads over extended periods across select ranges. These ranges reflect the gamut of business cases from regional flights (120–70 n miles) between closely spaced cities such as San Francisco and Sacramento, midrange (70–40 n miles) flights between polycentric cities like Dallas–Fort Worth, and short-range flights (40–10 n miles) within the cities themselves.

III. Electric UAM Aircraft Configurations

The four electric aircraft modeled in this study were an electric conventional takeoff and landing (ECTOL) aircraft, a stopped-rotor EVTOL aircraft, a tandem tilt-wing EVTOL aircraft, and a hexacopter EVTOL aircraft. Renderings of these vehicles are provided in Fig. 2. Their distinct configurations span the four major categories of aircraft envisioned to facilitate UAM. Inspiration for the aircraft was taken from NASA's X-57, Archer's Maker, Airbus's Vahana, and the now-retired CityAirbus concept, respectively. The ECTOL aircraft is a high-wing airplane with an engine (motor and rotor combination) mounted near the midspan on each wing. Due to the absence of vertical-lift rotors or fans, this aircraft requires takeoff field lengths that are two orders of magnitude

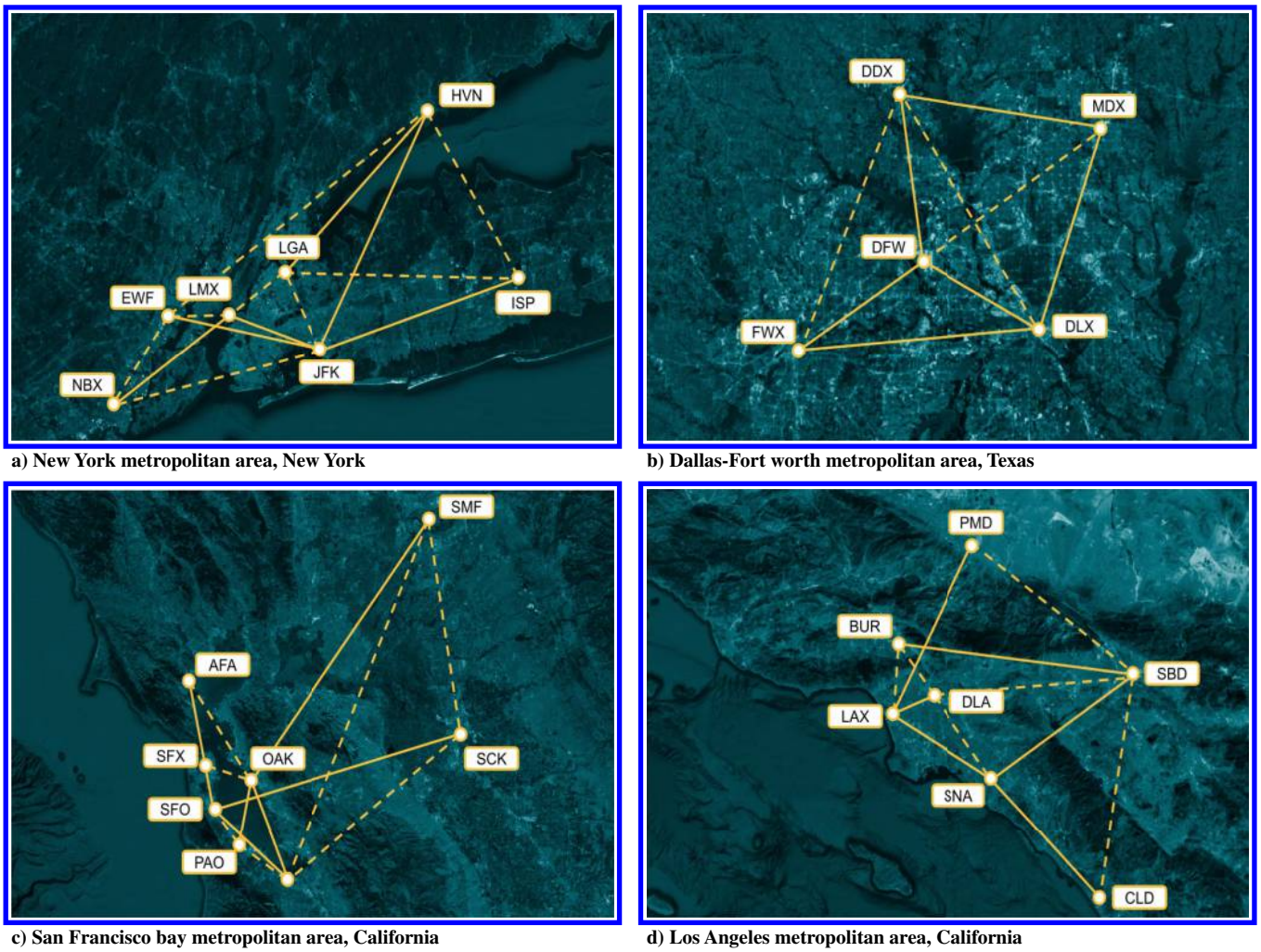

a) New York metropolitan area, New York

b) Dallas-Fort worth metropolitan area, Texas

c) San Francisco bay metropolitan area, California

d) Los Angeles metropolitan area, California

Fig. 1 Potential UAM routes in four major metropolitan areas within the United States.

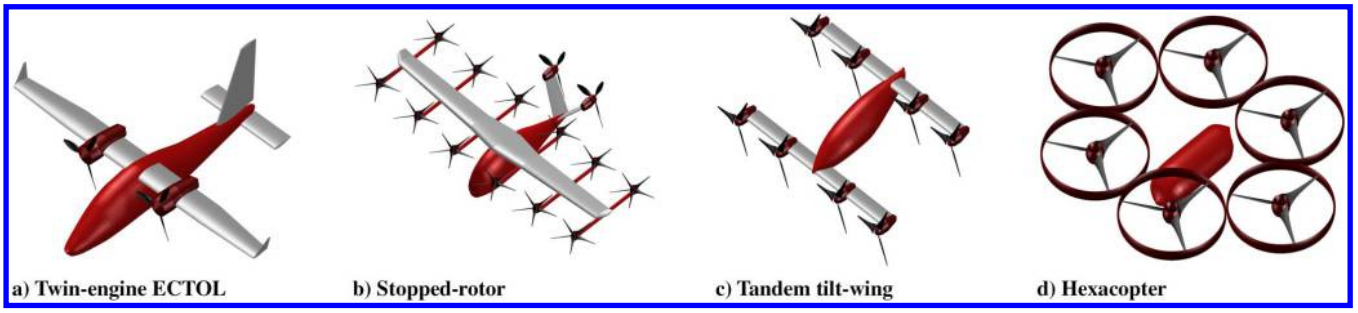

a) Twin-engine ECTOL b) Stopped-rotor c) Tandem tilt-wing d) Hexacopter

Fig. 2 Electric aircraft models.

greater than EVTOL aircraft, limiting its operation to standard airports with runways. On the other hand, the stopped rotor is of the lift+cruise EVTOL category and is characterized by separate powertrains for vertical climb and forward flight. The transition between hover and cruise is made possible through a combination of these separate propulsive systems. Estimating the electrical load drawn by the motors during the transitioning phases of flight is somewhat nontrivial, requiring medium- to high-fidelity computational methods to accurately predict the forces and moments about the vehicle's center of gravity. Next is the tandem tilt-wing aircraft of the vectored-thrust EVTOL type. The particular aircraft in this study possess eight engines, with four mounted on each the front canard wing and the main rear wing. Both wings, however, do have equivalent spans, aspect ratios, and tapers. This vehicle uses lifting surfaces and thrust vectoring to perform its transitioning maneuvers. Lastly, the hexacopter is a six-rotor multirotor EVTOL aircraft with engines mounted above the fuselage using struts (not modeled in the image).

Table 2 provides a high-level overview of each aircraft to facilitate the reproduction of findings presented in later sections of the paper. The aircraft are all designed to carry six passengers or an equivalent payload of 925 lb. Other geometric parametrizations are inspired by publicly available information about the reference aircraft. Documented in Ref. [14] are the semiempirical models that capture the impact of continuous cycling and environmental conditions experienced during flight. Because the battery pack modules are assumed to be air-cooled, a model of the ambient temperature is required. This was obtained from the National Centers for Environmental Information [20] for the San Francisco Bay metropolitan area. Within the modules, flow conditions are dominated by boundary-layer separation effects and wake interactions. The cells were therefore modeled as tube banks in a crossflow using empirical correlations outlined by

Table 2 Vehicle parameters

	ECTOL	Stopped rotor	Tandem tilt wing	Hexacopter
		General vehicle characteristics		
Capacity, passengers	6	6	6	6
Radial footprint, ft	36	48	32	39
Reference area, ft^2	159	180	234	96
TOGW, lb	3,947	6,113	6,007	8,381
Battery				
Pack capacity, kWh	92	179	249	631
Number of modules	10	10	10	10
Module geometric layout	$12\parallel \times 6 \perp$	$14\parallel \times 10 \perp$	$15\parallel \times 13 \perp$	$19\parallel \times 26 \perp$
Module electrical layout	12 s × 60 p	14 s × 100 p	15 s × 130 p	19 s × 260 p
Pack electrical layout	10 s × 1 p	10 s × 1 p	10 s × 1 p	10 s × 1 p
Powerplant				
Rotors	2 propellers	2 propellers12 rotors	8 rotors	6 rotors
Motors	2 × 83 kW motors	2 × 221 kW motors 12 × 47 kW motors	8 × 108 kW motors	6 × 155 kW motors
Propeller diameter, ft	6.3	7.5	— —	— —
Rotor diameter, ft	— —	7.5	7.9	16.4
		Performance		
Cruise speed, mph	175	175	175	75
Maximum operational altitude, ft	14,000	5,000	5,000	2,500

TOWG = Take-off gross weight.

Bergman et al. [21] to estimate the heat removed from the system. The size and breakdown of the battery packs are also documented in Table 2. Here, $\parallel$ represents the number of cells parallel to the cooling airflow, whereas $\perp$ represents the number of cells perpendicular to the cooling airflow with a module. The spacing between cells was set to 2 mm for all modules. The electrical circuit layouts at both the module and pack levels are also provided in Table 2. Here, "s" denotes the number of units (cells or modules) in series, and "p" denotes the number of units in parallel. Lastly, the SOH is assumed to be uniform across all cells in the battery pack. This, of course, is not the case in real life because, even with the aid of state-of-the-art quality control, new cells can vary ever so slightly. The responsibility of the battery management systems to balance the electrical load during discharging and charging becomes critical to ensuring that no one cell experiences loads beyond its manufacturer-rated limits. Powertrains of the aircraft were sized based on design loads computed through a physics-based component weight buildup approach documented by Smart and Alonso [22], thus guaranteeing that the aerodynamic and propulsion network analysis routines captured realistic estimates of flight load and energy consumption. A detailed description of vehicle sizing, weight breakdown, and the integrated multidisciplinary models used to assess performance can be found in previous work [23].

IV. Operational Lifetime Simulations

The open-source python-based code, SUAVE [24], is used to perform simulations. This platform was developed with modularity in mind, allowing design freedom in propulsion network modeling and the choice in the level of fidelity for analyzing both component-level and full-configuration performance. At each pseudospectral collocation point, the mission solver computed both dimensional quantities and nondimensional coefficients. In previous work [25], Clarke et al. demonstrated the importance of modeling the flight mechanics of all segments that define an aircraft's trajectory. For example, during the climb to cruising altitudes, nonlinear throttle profiles arise even in constant-speed flight segments by virtue of the aircraft flying through a varying density atmosphere. The instantaneous C rate also exhibits nonlinear behavior in constant power segments as the remaining energy in the battery depletes over time. This quantity paints a clearer picture of the battery cycle life than the more commonly used nominal C rate, which refers to the rate of discharge relative to a cell's nominal capacity. On the other hand, the instantaneous C rate is a measure of the cell's ability, at its current SOC, to supply the energy required by the motors. This observability becomes increasingly important near the end of the cycle when the cell reaches the knee point on the SOC curve, and any loads past this point will see a drastic drop in performance.

The flight profile of each aircraft is detailed in Table 3, with a more descriptive summary of rigid-body kinematics provided in Table 4. The specific values used in the simulation of each flight profile (including the altitude, airspeed, climb rate, rotor orientation angle, and pitch command for each segment for each aircraft) were provided in the appendix of Ref. [26]. A comparison of the aerodynamic, acoustic, and powertrain performances of these for aircraft flying their respective flight profiles was documented by Clarke and Alonso [23], and thus the authors choose to refer readers to that study.

Detailed in Table 5 are the nine ranges each aircraft is simulated through, with all processing similar climb and descent segments; only the cruise segment is modified. As shown in the table, the distances of hexacopter ranges are well below that of the other three aircraft, underscoring this vehicle's inability to perform long-range flight operations. This is due to the large amounts of power required by this configuration to perform cruises without the benefit of wings

Table 3 Aircraft flight segments

Segment	Twin-engine ECTOL	Stopped rotor	Tilt wing	Hexacopter
1	Takeoff	Vertical climb	Vertical climb	Vertical climb
2	Departure end of runway	Vertical transition	Vertical transition	Vertical transition
3	Initial climb area	Climb transition	Climb transition 1	Climb
4	Climb	Climb 1	Climb transition 2	Cruise
5	Cruise	Climb 2	Climb	Descent
6	Descent	Cruise	Cruise	Descent transition
7	Downleg	Descent	Descent	Vertical descent
8	Base leg	Approach transition	Approach transition	— —
9	Final approach	Descent transition	Descent transition	— —
10	Landing	Vertical descent	Vertical descent	— —

Table 4 Flight segment kinematics

Segment	Symbol	Segment kinematics
Approach transition	AT	Constant acceleration/constant angle/linear climb
Base leg	BL	Linear speed/constant rate
Climb	CL	Linear speed/constant rate
Climb transition	CT	Constant acceleration/constant angle/linear climb
Cruise	CR	Constant speed/constant altitude
Departure end of runway	DER	Linear speed/constant rate
Descent	D	Linear speed/constant rate
Descent transition	DT	Constant acceleration/constant pitch rate/constant altitude
Downleg	DL	Constant acceleration/constant altitude
Final approach	FA	Linear speed/constant rate
Initial climb area	ICA	Linear speed/constant rate
Vertical climb	VC	Vertical ascent
Vertical transition	VT	Constant acceleration/constant pitch rate/constant altitude
Vertical descent	VD	Vertical descent

Table 5 Simulated ranges of the electric aircraft

	Range, n miles								
Aircraft	Case 1	Case 2	Case 3	Case 4	Case 5	Case 6	Case 7	Case 8	Case 9
Twin-engine ECTOL	60	65	70	75	80	85	90	95	100
Stopped-rotor EVTOL	60	65	70	75	80	85	90	95	100
Tilt-wing EVTOL	60	65	70	75	80	85	90	95	100
Hexacopter EVTOL	20	22.5	25	27.5	30	32.5	35	37.5	40

that enable efficient long-range flight. Lastly, eight daily flights reflect the continuous services that UAM businesses are expected to operate. Recharging at 1 C from the end-of-flight SOC to 100% SOC was also simulated after each flight. This, of course, does not necessarily mean that the battery reaches the same capacity as its pristine state because the cell ages with time.

V. Time-Dependent Aircraft Performance over Operational Lifetime Diagrams

Simulating extended periods of time presents two unique challenges: representing large amounts of information and determining how best to weigh the various aspects of vehicle performance. On top of this, with the incorporation of temperature as a function of both altitude and time of year, some observations exhibit strong bivariance. We therefore rely on TAPOOL diagrams to describe the behavior of an electric aircraft's battery pack under realistic flight and environmental conditions. This differs from traditional approaches to assessing battery-powered aircraft in two ways: first, time dependency is introduced into the efficiency criteria of stored-energy systems; and second, the entire flight profile, which includes the climb and descent stages of a mission, is used rather than the constant altitude and constant airspeed assumptions in the computation of range and endurance.

The battery's performance in any given flight segment is also directly affected by its history, or rather the electrical load that pack was subjected to during the previous segment. This meant that simulations had to be performed in sequence and computational operations could not be parallelized. Depending on the aircraft configuration, simulations therefore took between two and five days on a single node on the in-house eight-node cluster of the Aerospace Design Laboratory at Stanford University. Hence, the data presented in the study were amassed over a period of one month. This, however, is still significantly shorter than running capacity tests on cells within a laboratory setting on a programmable cycler. By and large, leveraging computer simulations has the potential to 1) fill the gaps of experimental data, 2) accelerate testing by addressing the information entropy problem (that is, determining the least amount of information required to characterize cell aging fully), and 3) predict battery end of life. The following subsections discuss the TAPOOL diagrams for the battery cell capacity, maximum cell temperature, and maximum instantaneous C rate. These three variables were deemed to be the most significant, given their implications on both safety and performance at the system level. In the following figures, simulations are terminated when the SOC at the end of a flight first reaches a lower threshold of 20%, signifying the end of useful life. The decision to use this cutoff value over other thresholds of 15% and even 10% (suggested by German et al. [27]) was because, as the cell degrades, the inflection point where there is a precipitous drop in voltage becomes increasingly tricky to predict in practice. The higher cutoff SOC therefore ensures that the simulated operations will be guaranteed. Infeasible regions of flight missions are hashed in black and white on the figures.

A. Battery Capacity

Arguably the most important metric in the cell SOH, capacity fade is a measure of the change in the cell's charge-storing potential relative to its pristine condition at the beginning of use. This degradation can be credited to several internal mechanisms, including the deterioration of the rock salt structure of the cathode; exfoliation of the graphite structure at the anode, resulting in a weakening of bonding potential; and the growth of the SEI layer that consumes active material. Figure 3 depicts the behavior of capacity fade as a function of the range and number of days in operation. As expected, the general trend across configurations is that longer missions accelerate cell degradation and reduce the operational lifetime. In other words, the number of days that a particular aircraft can fly a given route decreases with increasing cruise distance. For the flight schedules defined in the previous section, it was observed that the battery life of achievable missions can drop by as much as 45% by the end of a calendar year, depending on the vehicle configuration, range, and battery pack size. From a purely utilitarian standpoint, the ECTOL aircraft, with the highest operational periods across all ranges, is the most energy-efficient option. This, however, does not factor in the footprint needed for takeoff by such a configuration, which poses a significant dilemma for operating in urban spaces. Taking a step back to assess the implications of these trends on vehicle choice, we see from a graphical analysis that the lifetimes of operation of ECTOL, stopped-rotor EVTOL, tilt-wing EVTOL, and hexacopter EVTOL aircraft decrease by 11, 8, 9, and 23 days, respectively, for every additional nautical mile flown. These linearized approximations were computed by examining end-of-life states at the 90- and 70-n-mile ranges for the first three vehicles and 37.5 and 30 n miles for the hexacopter. It is important to note that these rates are not necessarily a comparison of energy consumption in the respective battery packs but rather the rate at which this energy depletes. These rates do, however, provide direction in constructing more appropriately sized battery packs. The preceding plots also lend key insights into what strategies air-shuttle and air-taxi services should adopt to maximize the potential of both brand-new and used aircraft. Taking San Francisco, for example, we can infer from Fig. 3a that a service using a new twin-engine ECTOL aircraft between Oakland

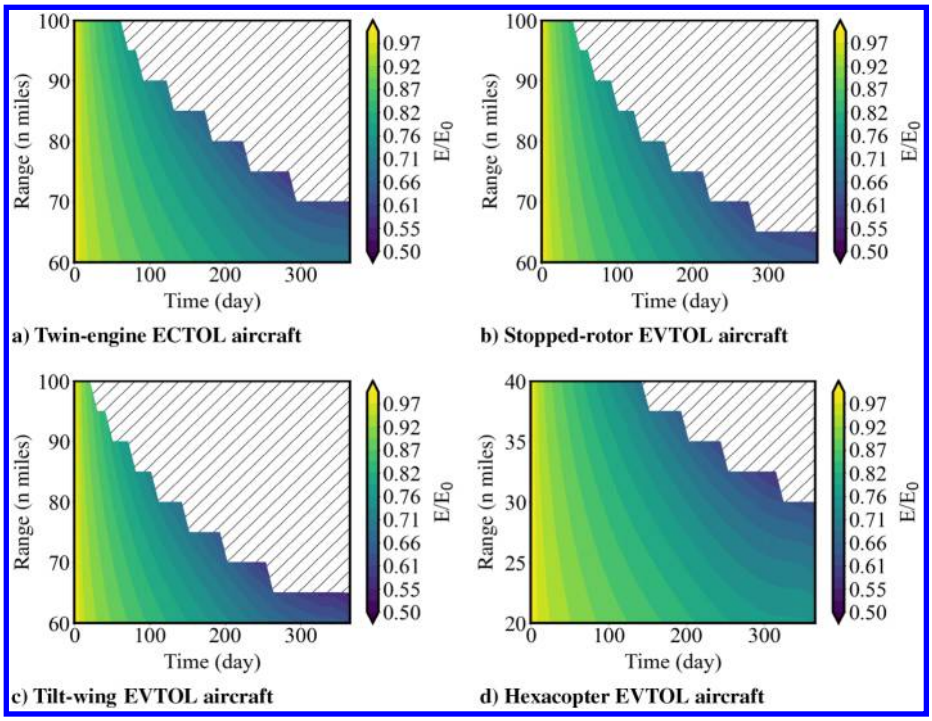

Fig. 3 Cell capacity TAPOOL contours.

International Airport (OAK) and Sacramento International Airport (SMF) will last around 200 days. As another example, using Fig. 3d, we can arrive at a service period of 350 days for a hexacopter operating nonstop between Norman Y. Mineta San Jose International Airport (SJC) and either OAK or San Francisco International Airport (SFO), which are roughly the same distance apart. On the other hand, if we have a tilt-wing EVTOL that has been providing a 90-n-mile regional service in the New York Metropolitan Area between Philadelphia International Airport (PHL) (not shown in Fig. 1a) and lower Manhattan for 100 days, it can be repurposed for flights between John F. Kennedy International Airport (JFK) and Long Island MacArthur Airport (ISP) to extend the service life by another 200 days before battery pack replacement is needed. It must be stated here, however, that empirical-based models for prediction of the SOH have been known to exhibit poor extrapolation behavior. It is therefore recommended that modelers solely perform interpolation within a simulated range to guarantee low uncertainty.

B. Maximum Instantaneous C Rate

Shown in Fig. 4 are the changes in current severity passing through a particular cell at any given instant in time. Before we elaborate on these trends, it is important to first remind readers of the terminology concerning C rate used in this study. Continuing the discussion in Sec. IV, a nominal C rate can be viewed as the current through the

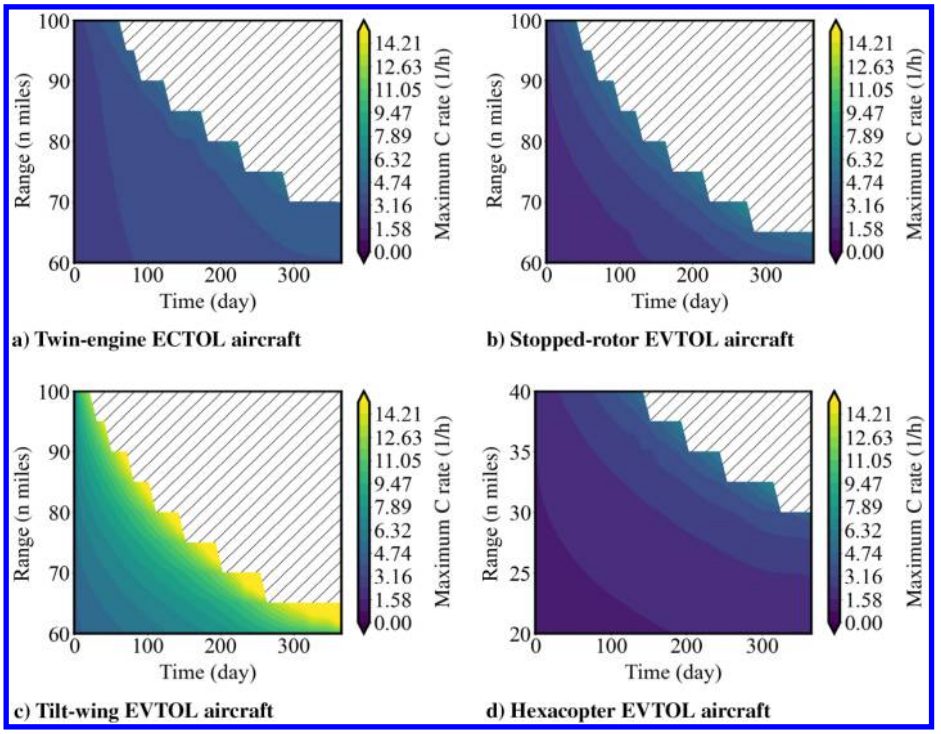

Fig. 4 Maximum instantaneous C-rate TAPOOL contours.

battery divided by the current draw under which the battery would deliver its rated capacity in 1 h. For example, a discharge of 2 C of a 1 Ah cell indicates that the cell would be fully discharged in 30 min. This rated capacity is typically provided by the manufacturer but can be experimentally determined in the laboratory [28]. Conversely, in this study, we use the instantaneous C rate, which is defined as the rate at which a battery is being discharged relative to the cell's capacity at that current state in time. This was the preferred metric because it allowed us to understand the differences between discharges of equivalent magnitude at opposite ends of the SOC range: that is, fully charged and fully discharged. The instantaneous C rate conveys how severe discharges near the end of cycle are to battery health.

As the battery ages and the voltage (as a function of the SOC) drops, more current is required to supply the same power to the powertrain. The maximum C rates for the four aircraft therefore all increase with an increasing range and length of operation. We can also deduce from Fig. 4c that despite the battery pack of the tilt-wing EVTOL aircraft being sized to meet mission specifications at the beginning of service, the electrical layout (number of cells in series and parallel) was not copiously done, resulting in extremely high C rates as time progressed. These trends could not have been observed in a single-flight analysis, further demonstrating the versatility of TAPOOL diagrams.

C. Maximum Cell Temperature

Accompanying the increase in ohmic resistance within the battery cell is the increase in temperature. Unlike the prior two quantities discussed earlier in this paper, the heat generated by the cells over the aircraft's operational lifetime exhibits strong bivariance because its behavior is somewhat offset by the ambient temperature, which changes year round. For example, if we examine a 65-n-mile mission of the twin-engine ECTOL aircraft in Fig. 5a, we witness that during the months of August and September, the temperature within the battery module can reach 318 K or 45°C. In longer-range missions, temperatures can even reach 324 K or 50°C earlier in the year as a result of a rise in accumulated heat energy during cruise segments of the flight profile. This temperature increase is a direct result of the constant airflow of the cooling air in the simulations, which governs heat rejection. Generally speaking, all electrochemical cells have an optimum temperature range of operation: lithium-ion battery cells included. Operating within this window not only guarantees that the battery performs at its full potential but prolongs the life of the cell. The temperature TAPOOL diagram hence provides system designers with critical insights into the design of the thermal management system and the cell layout needed to achieve ideal operating conditions within the module.

VI. Comparison with Traditional Electric Aircraft Performance Metrics

Early studies by Retana and Rodriguez-Cortes [29] and Lawrence and Mohseni [30] paved the way for the widely used formulations by Traub [31] for estimating the range and endurance of battery-powered aircraft. These formulations start with the simple energy balance in Eq. (1a), in which the power required for steady, level flight is balanced with the speed and drag of the aircraft. As shown in Eq. (1b), the drag force can be further deconstructed into its zero-lift component, which captures the profile drag and skin friction, as well as the drag due to lift, which is corrected by a factor to account for aerodynamic phenomena such as viscous pressure drag and vortex drag. With suitable substitutions to express lift in terms of the vehicle weight, lift coefficient, and wing area, the required power can be expressed as the product of the drag force D and airspeed U:

$$P_{\text{req}} = D * U = \frac{1}{2}\rho U^2 S C_D * U \tag{1a}$$

$$C_D = C_{D_0} + kC_D^2 \tag{1b}$$

$$P_{\text{req}} = \frac{1}{2}\rho U^2 S C_{D_0} + \frac{2W^2 k}{\rho U S} \tag{1c}$$

In steady, continuous flight, this power is balanced by that supplied by the battery given by

$$P_{\text{bat}} = V * i \tag{2}$$

that, by using a modification of Peukert's equation in Eq. (3) for the current of an electrochemical cell, can be expressed as

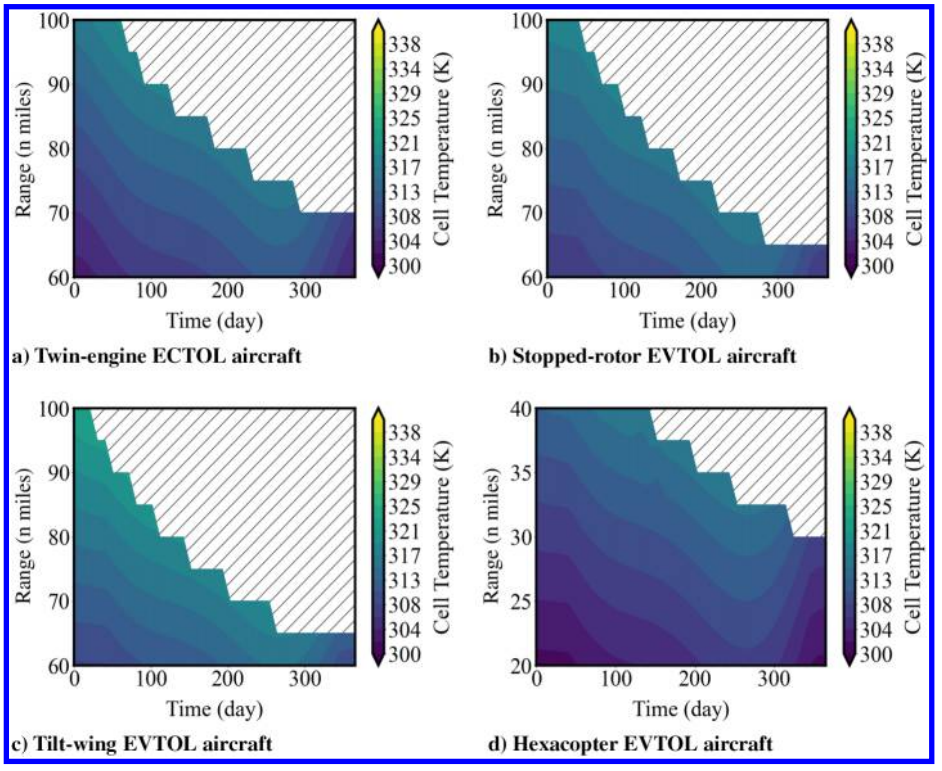

Fig. 5 Maximum temperature TAPOOL contours.

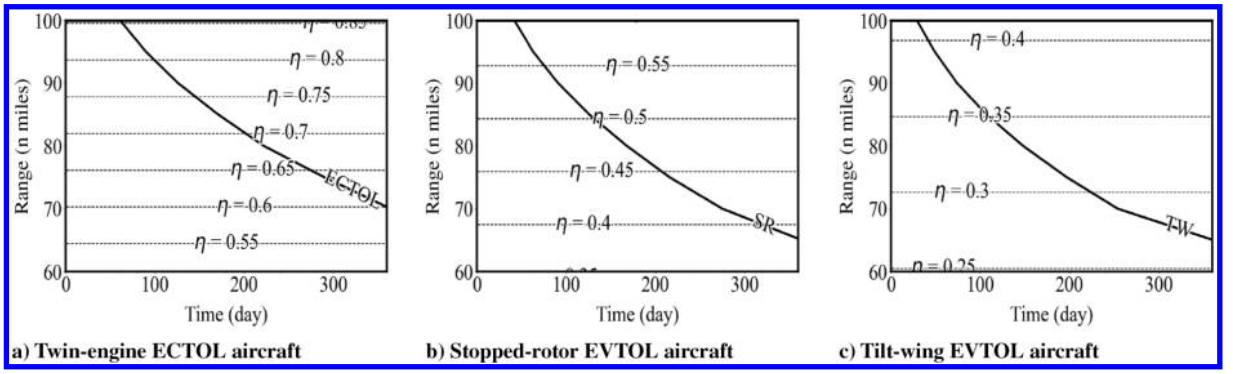

Fig. 6 Comparison of aircraft endurance trends using battery degradation modeling and traditional electric range equation.

$$i^n = \frac{Rt}{t}\left(\frac{C}{Rt}\right)^n \tag{3}$$

which is given by

$$P_{\text{bat}} = V * \frac{Rt}{t}\left(\frac{C}{Rt}\right)^n \tag{4}$$

Here, V is the voltage, Rt is the hour rating, C is the battery capacity in ampere hours, i is the discharge current, and n is a hyperparameter that accounts for the physical properties of the cell as well as its operating conditions. It is important to note here that this is but one of the many proposed expressions to represent the available electrical load on discharge, which is oftentimes chosen due to its ease of implementation. More accurate methods worth mentioning for estimating the current drawn at a particular SOC include higher-fidelity physics-based methods such as the pseudo-two-dimensional or porous electrode diffusion models and medium-fidelity methods such as the equivalent circuit model used in this study.

Through energy balance of the system, Eqs. (1c) and (4) can be rearranged to obtain the endurance t given as

$$t = Rt^{1-n}\left[\frac{\eta_{\text{tot}} VC}{(1/2)\rho U^3 S C_{Do} + (2W^2 k/\rho US)}\right]^n \tag{5}$$

where η_{tot} is the combined efficiency of the system subcomponents. A simpler form of this expression can be obtained without the decomposition of drag into its components and using the assumption that V is the nominal voltage, allowing the substitution for battery energy of $E = VC$, and the assumption that $n = 1$:

$$t = \eta_{\text{tot}} \frac{E^L/_D}{WU} \tag{6}$$

where η_{tot} is the combined system efficiency; L/D is the lift-to-drag ratio at steady, level flight; and E is the available energy, which is taken as 80% to the total energy of the pack. We can use Eq. (6) to compare this traditional approach for estimating endurance to the findings in this paper. Shown in Fig. 6 is the maximum achievable range for three of the four aircraft, which is superimposed with trendlines corresponding to different system efficiencies. The stopped-rotor and tilt-wing EVTOL aircraft are abbreviated SR and TW in Figs. 6b and 6c respectively. Notwithstanding the constant airspeed and altitude assumption, a noticeable disparity in performance can be observed as the battery pack ages. Moreover, we see that for the two EVTOL aircraft in Fig. 6b and 6c, the low system efficiencies bisecting the aircraft limits predicted by the model suggest that the use of traditional approaches is not suitable for estimating endurance. That said, it must be acknowledged that the simplified equations derived in this section are often used for "back of the envelope"-type analyses and still have value in early-stage conceptual design. In contrast, the developed method used to construct TAPOOL diagrams takes weeks to generate results. There is, therefore, a time and place for both.

VII. Conclusions

Any comprehensive assessment of the performance of stored-energy systems such as battery-powered aircraft must involve incorporating time-dependent factors that capture the reduction in efficiency with repeated use. This paper demonstrates the application of lithium-ion degradation models to studying aircraft performance: specifically, flight operations symbolizing regional and urban air mobility commuting. The findings of this study suggest that after a year of continuous operation, albeit excessive in terms of the number of flights per day, it can reduce battery capacity by as much as 45%. The TAPOOL diagrams can also provide high-level insights on the impact of increasing propulsive and aerodynamic efficiency. More specifically, for the aircraft with VTOL capability, reducing power loading will reduce both electrical and thermal stresses incurred by the battery cell during the hover and transition stages of flight. Furthermore, for the winged aircraft in cruise, reducing drag will have a noticeable effect on capacity fade; low C rates during cruises lead to marginal thermal loads. In so doing, such diagrams shed light on potential research and development areas like battery inverse design, in which lithium-ion battery cells can be tailored for aerospace applications. This allows them to handle the high C-rate discharges during the beginning and end of cycle life. Other areas of improvement at the module level include developing more robust thermal management system algorithms, given that thermal loads can now be predicted. Finally, at the systems level, the findings of this study present the opportunity to conceptualize flight operation strategies to maximize vehicle life before significant ground maintenance is needed.

References

[1] Zhang, C., Yan, F., Du, C., Kang, J., and Turkson, R. F., "Evaluating the Degradation Mechanism and State of Health of LiFePO4 Lithium-Ion Batteries in Real-World Plug-In Hybrid Electric Vehicles Application for Different Ageing Paths," *Energies*, Vol. 10, No. 1, 2017, Paper 37. https://doi.org/10.3390/en10010110

[2] Cordoba-Arenas, A., Onori, S., Guezennec, Y., and Rizzoni, G., "Capacity and Power Fade Cycle-Life Model for Plug-In Hybrid Electric Vehicle Lithium-Ion Battery Cells Containing Blended Spinel and Layered-Oxide Positive Electrodes," *Journal of Power Sources*, Vol. 278, March 2015, pp. 473–483. https://doi.org/10.1016/j.jpowsour.2014.12.047

[3] Han, X., Ouyang, M., Lu, L., Li, J., Zheng, Y., and Li, Z., "A Comparative Study of Commercial Lithium Ion Battery Cycle Life in Electrical Vehicle: Aging Mechanism Identification," *Journal of Power Sources*, Vol. 251, April 2014, pp. 38–54. https://doi.org/10.1016/j.jpowsour.2013.11.029

[4] Yan, D., Lu, L., Li, Z., Feng, X., Ouyang, M., and Jiang, F., "Durability Comparison of Four Different Types of High-Power Batteries in HEV and Their Degradation Mechanism Analysis," *Applied Energy*, Vol. 179, Oct. 2016, pp. 1123–1130. https://doi.org/10.1016/j.apenergy.2016.07.054

[5] Isikveren, A. T., Pornet, C., Vratny, P. C., and Schmidt, M., "Optimization of Commercial Aircraft Using Battery-Based Voltaic-Joule/Brayton Propulsion," *Journal of Aircraft*, Vol. 54, No. 1, 2017, pp. 246–261. https://doi.org/10.2514/1.C033885

[6] De Vries, R., Brown, M., and Vos, R., "Preliminary Sizing Method for Hybrid-Electric Distributed-Propulsion Aircraft," *Journal of Aircraft*, Vol. 56, No. 6, 2019, pp. 2172–2188. https://doi.org/10.2514/1.C035388

[7] Finger, D. F., Bil, C., and Braun, C., "Initial Sizing Methodology for Hybrid-Electric General Aviation Aircraft," *Journal of Aircraft*, Vol. 57, No. 2, 2020, pp. 245–255. https://doi.org/10.2514/1.C035428

[8] Moore, K. R., and Ning, A., "Takeoff and Performance Trade-Offs of Retrofit Distributed Electric Propulsion for Urban Transport," *Journal of Aircraft*, Vol. 56, No. 5, 2019, pp. 1880–1892. https://doi.org/10.2514/1.C035321

[9] Ma, Y., Zhang, W., Zhang, Y., Zhang, X., and Zhong, Y., "Sizing Method and Sensitivity Analysis for Distributed Electric Propulsion Aircraft," *Journal of Aircraft*, Vol. 57, No. 4, 2020, pp. 730–741. https://doi.org/10.2514/1.C035581

[10] Traub, L. W., "Optimal Battery Weight Fraction for Maximum Aircraft Range and Endurance," *Journal of Aircraft*, Vol. 53, No. 4, 2016, pp. 1177–1179. https://doi.org/10.2514/1.C033416

[11] Hamilton, T., and German, B. J., "Optimal Airspeeds for Scheduled Electric Aircraft Operations," *Journal of Aircraft*, Vol. 56, No. 2, 2019, pp. 545–555. https://doi.org/10.2514/1.C035051

[12] Isikveren, A. T., "Method of Quadrant-Based Algorithmic Nomographs for Hybrid/Electric Aircraft Predesign," *Journal of Aircraft*, Vol. 55, No. 1, 2018, pp. 396–405. https://doi.org/10.2514/1.C034355

[13] Finger, D. F., Braun, C., and Bil, C., "Case Studies in Initial Sizing for Hybrid-Electric General Aviation Aircraft," *2018 AIAA/IEEE Electric Aircraft Technologies Symposium (EATS)*, Inst. of Electrical and Electronics Engineers, New York, 2018, pp. 1–22.

[14] Clarke, M., and Alonso, J. J., "Lithium–Ion Battery Modeling for Aerospace Applications," *Journal of Aircraft*, Vol. 58, No. 6, Nov. 2021, pp. 1323–1335.

[15] Reiche, C., Goyal, R., Cohen, A., Serrao, J., Kimmel, S., Fernando, C., and Shaheen, S., "Urban Air Mobility Market Study," NASA TR HQ-E-DAA-TN65181, 2018, pp. 1–163, https://ntrs.nasa.gov/citations/20190001472 [retrieved 14 Nov. 2021].

[16] Goyal, R., Reiche, C., Fernando, C., and Cohen, A., "Advanced Air Mobility: Demand Analysis and Market Potential of the Airport Shuttle and Air Taxi Markets," *Sustainability*, Vol. 13, No. 13, 2021, Paper 7421. https://doi.org/10.3390/su13137421

[17] Mayor, T., and Anderson, J., "Getting Mobility Off the Ground," KPMG International, Zurich, Switzerland, 2019, https://institutes.kpmg.us/content/dam/advisory/en/pdfs/2019/urban-air-mobility.pdf [retrieved 18 Nov. 2021].

[18] Robinson, J. N., Sokollek, M.-D. R., Justin, C. Y., and Mavris, D. N., "Development of a Methodology for Parametric Analysis of STOL Airpark Geo-Density," *2018 Aviation Technology, Integration, and Operations Conference*, AIAA Paper 2018-3054, 2018.

[19] Antcliff, K. R., Moore, M. D., and Goodrich, K. H., "Silicon Valley as an Early Adopter for On-Demand Civil VTOL Operations," *16th AIAA Aviation Technology, Integration, and Operations Conference*, AIAA Paper 2016-3466, 2016.

[20] Daily Summaries Location Details, online database, National Oceanic and Atmospheric Administration, National Centers for Environmental Information, Silver Spring, MD, https://www.ncdc.noaa.gov/cdo-web/datasets/GHCND/locations/CITY:US060031/detail [retrieved 02 Nov. 2019].

[21] Bergman, T. L., Incropera, F. P., and DeWitt, D. P., andLavine, A. S., *Fundamentals of Heat and Mass Transfer*, Wiley, Hoboken, NJ, 2011, pp. 436–447.

[22] Smart, J. T., and Alonso, J. J., "Primary Weight Estimation for eVTOLs via Explicit Analysis and Surrogate Regression," AIAA Paper 2019-3679, June 2019, pp. 1–12. https://doi.org/10.2514/6.2019-3679

[23] Clarke, M. A., and Alonso, J., "Evaluating the Performance and Acoustic Footprint of Aircraft for Regional and Urban Air Mobility," *AIAA Aviation 2021 Forum*, AIAA Paper 2021-3205, 2021b.

[24] Botero, E., Clarke, M., Erhard, R., Smart, J., MacDonald, T., Vegh, J. M., Lukaczyk, T., da Silva, C. R. I., Momose, T., Blaufaux, A., Orra, T., and Wendorff, A., suavecode/SUAVE: SUAVE 2.5.0, Software Package, Stanford Univ., Stanford, CA, 2021. https://doi.org/10.5281/zenodo.5661107

[25] Clarke, M., Smart, J., Botero, E., Maier, W., and Alonso, J., "Strategies for Posing a Well-Defined Problem for Urban Air Mobility Vehicles," *AIAA SciTech 2019 Forum*, AIAA Paper 2019-0818, 2019. https://doi.org/10.2514/6.2019-0818

[26] Clarke, M. A., and Alonso, J. J., "Forecasting the Operational Lifetime of Electric Aircraft Through Battery Degradation Modeling," *AIAA SciTech 2022 Forum*, AIAA Paper 2022-1996, 2022.

[27] German, B., Daskilewicz, M., Hamilton, T. K., and Warren, M. M., "Cargo Delivery in by Passenger eVTOL Aircraft: A Case Study in the San Francisco Bay Area," *2018 AIAA Aerospace Sciences Meeting*, AIAA Paper 2018-2006, 2018. https://doi.org/10.2514/6.2018-2006

[28] Christophersen, J. P., *Battery Test Manual for Electric Vehicles*, Rev. 3, Idaho National Lab., Idaho Falls, ID, 2015, p. 5.

[29] Retana, E. R., and Rodriguez-Cortes, H., "Basic Small Fixed Wing Aircraft Sizing Optimizing Endurance," *2007 4th International Conference on Electrical and Electronics Engineering*, Inst. of Electrical and Electronics Engineers, New York, 2007, pp. 322–325.

[30] Lawrence, D., and Mohseni, K., "Efficiency Analysis for Long Duration Electric MAVs," *AIAA Infotech@Aerospace*, AIAA Paper 2005-7090, Sept. 2005. https://doi.org/10.2514/6.2005-7090

[31] Traub, L. W., "Range and Endurance Estimates for Battery-Powered Aircraft," *Journal of Aircraft*, Vol. 48, No. 2, 2011, pp. 703–707. https://doi.org/10.2514/1.C031027